

Epitaxy of Fe_3O_4 on Si(001) by pulsed layer deposition using a TiN/MgO buffer layer

D. Reisinger,^{1,*} M. Schonecke,¹ T. Brenninger,¹ M. Opel,¹ A. Erb,¹ L. Alff,^{1,†} and R. Gross¹

¹Walther-Meißner-Institut, Bayerische Akademie der Wissenschaften,
Walther-Meißner Str. 8, 85748 Garching, Germany

(Dated: received December 24, 2002)

Epitaxy of oxide materials on silicon (Si) substrates is of great interest for future functional devices using the large variety of physical properties of the oxides as ferroelectricity, ferromagnetism, or superconductivity. Recently, materials with high spin polarization of the charge carriers have become interesting for semiconductor-oxide hybrid devices in spin electronics. Here, we report on pulsed laser deposition of magnetite (Fe_3O_4) on Si(001) substrates cleaned by an *in situ* laser beam high temperature treatment. After depositing a double buffer layer of titanium nitride (TiN) and magnesium oxide (MgO), a high quality epitaxial magnetite layer can be grown as verified by RHEED intensity oscillations and high resolution x-ray diffraction.

PACS numbers: 61.14.Hg, 75.70.-i, 81.15.Fg

INTRODUCTION

Oxide thin films offer a large variety of physical properties useful for future electronic devices. Much attention has been paid to the ferroelectric, dielectric, and optical properties of perovskite materials with respect to non-volatile memory transistor applications or nonlinear optical devices [1]. In the area of so-called spintronics, ferromagnetic oxides with high spin polarisation P of the charge carriers at room temperature are desired for spin injection semiconductor devices as for example described by Datta and Das [2]. While it has been shown that the spin lifetime in semiconductors is high as compared to metals [3], one of the largest problems is to create a spin polarized population of the charge carriers in the semiconductor by injection of spin polarized currents. The use of diluted magnetic semiconductors - if existent - is possible but limited due to the low Curie temperatures of the magnetic semiconductors so far [4, 5]. Therefore, half-metallic materials with a full spin polarization of the charge carriers at the Fermi level and Curie temperatures well above room temperature are under consideration for spintronic devices. There are several candidates for materials with large P close to 100% such as the Mn-based Heusler alloys, the oxide ferromagnets such as Fe_3O_4 [6] or CrO_2 , the doped manganites, and also the double perovskites [7]. We note that the use of these materials for ferromagnet-semiconductor hybrid devices requires the epitaxial growth of these materials on semiconductors. This is a great challenge with respect to materials technology. We further note that the resistivity mismatch between ferromagnetic metals and the semiconductors puts fundamental limits on the degree of spin polarization achievable with spin injection [8]. The efficiency of spin injection, however, can be largely increased by introducing a tunnel barrier between the ferromagnetic metal and the semiconductor [9, 10].

Here, we report on the fabrication and structural characterization of magnetite (Fe_3O_4) epitaxial thin films on Si(001) substrates using a double buffer layer of TiN

and MgO. MgO is also a candidate for an insulating barrier required for future tunneling injection devices. An important step is the in-situ substrate treatment by an infrared laser beam heating system. This allows for the controlled removal of the amorphous Si oxide surface layer prior to film deposition monitored by reflection high energy electron diffraction (RHEED). After substrate cleaning, the thin films are grown by ultra high vacuum (UHV) laser molecular beam epitaxy (L-MBE) [11, 12]. Also, the complete growth process is monitored by RHEED. We discuss in detail the growth of the buffer layer system consisting of TiN and MgO matching the magnetite lattice constants, and the epitaxial growth of Fe_3O_4 on top of the buffer layer system. The surface of the completed Fe_3O_4 thin films as well as the developing heterostructures is characterized after each process step by *in situ* atomic force microscopy (AFM). The structural properties of the completed hybrid heterostructures have been investigated by high-resolution x-ray diffraction (HRXRD).

EXPERIMENTAL TECHNIQUES

The heteroepitaxial thin film structures have been grown using laser molecular beam epitaxy (L-MBE) [11, 12]. The thin film UHV system consists of three separate sub-chambers for pulsed laser deposition, metallization, surface analysis and a load-lock. A sketch of the sub-chamber for the pulsed laser deposition (PLD) is shown in Fig. 1. A technical description of the systems has been given recently [11, 12]. Therefore, we only discuss those parts of the system relevant for the work reported here. For the present study, the two most important parts are (i) the (high-pressure) RHEED system and (ii) the infrared laser heating system used for the substrate heating.

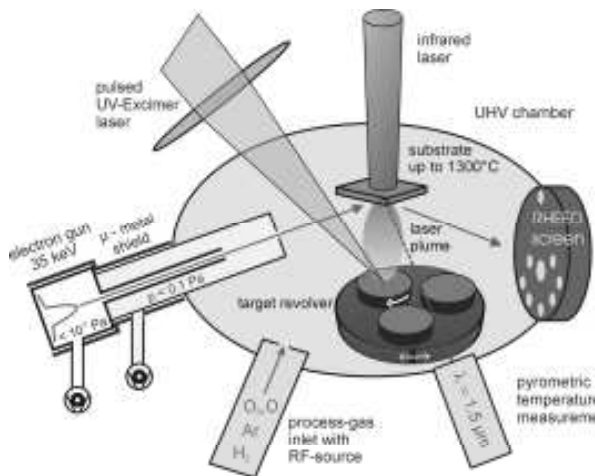


Figure 1: Sketch of the pulsed laser deposition chamber including the infrared laser heating system.

High pressure RHEED system

Many oxide materials have to be grown in a large oxygen partial pressure perturbing the RHEED analysis during growth due to the strong scattering of the high energy electrons from the oxygen molecules. Therefore, a special high pressure RHEED system has to be used, where the electrons travel only a short distance in the high pressure deposition atmosphere, and the rest of the beam path is pumped differentially [13]. In our system a double differential pumping unit is used allowing for the operation of the RHEED system up to pressures of several 10 Pa (for details see Ref. [12]).

Laser heating of Si(001) substrates

An infrared laser heating system to heat substrates in a thin film deposition system to temperature above 1200°C has first been introduced by Ohashi *et al.* [14]. Such a system has several advantages with respect to thin film epitaxy. First, inside the vacuum chamber of the deposition system the substrate is heated directly by the infrared laser positioned outside the vacuum system. Therefore, the substrate heating is more efficient than in the case of a radiation heater positioned inside the vacuum chamber. In particular, the use of a radiation heater results in parts with a temperature well above the substrate temperature located inside the vacuum system. This in turn usually results in reduced vacuum conditions. In our case, using the infrared laser heating a substrate temperature T_S well above 1200°C can be reached at a vacuum in the 10^{-8} mbar range. Compared to the radiation heater setup in the same chamber, an improvement of the background pressure of about an order of

magnitude is achieved. Second, the laser heating system allows for rapid changes of the substrate temperature, since only the substrate is heated, which has a much smaller heat capacity than the system radiation heater plus substrate. We realized changes of up to 500 K/min, only limited by the mechanical stability of the used substrate. Third, high temperatures up to the melting point of Si at 1410°C can be reached without using an extensive amount of radiation shielding preventing the optical access to the sample surface.

In our setup the beam of a diode laser with a wavelength of 950 nm and a maximum power of 100 W is fed through an optical viewport and directly irradiates the backside of the Si(001) substrate. Using transparent substrates like SrTiO_3 , one has to take into account the temperature dependence of the absorption coefficient η . Here, a small amount of silver paint on the backside of the substrate is sufficient to absorb most of the laser power. This allows for the increase of the substrate temperature to values, where η increases and thus enables substrate temperatures up to 1200°C. In contrast, Si has high infrared absorption already at room temperature and therefore does not require any backside treatment. For temperature measurement a high resolution pyrometer working at the wavelength of $1.5 \mu\text{m}$ is used. The measured spot size is only 1 mm^2 , so even temperature inhomogeneities on the small substrates can be detected. Changes in the emission coefficient ε of the substrates at the measuring wavelength give an error in true temperature. Calibration measurements in an oven showed that this error with a big change in ε of 0.25 (worst case scenario) is only about $\pm 3 \text{ K}$ at 400°C and $\pm 20 \text{ K}$ at 1000°C. We note, however, that the for the deposition processes important reproducibility of the deposition temperature is with 5 K on the used substrates much better. Compared to a thermocouple the absolute exactness of this pyrometric measurement is good and the reproducibility strongly improved.

In the following we discuss the cleaning process for the surface of the Si(001) substrates. In our work we used commercial Si(001) single crystal wafers, which are one side polished and cut into 5 mm by 5 mm pieces. These pieces have been precleaned in acetone and isopropanol using an ultrasonic bath. However, it is unavoidable that a thin amorphous silicon oxide layer forms on the substrate surface. For the epitaxial growth of a thin film structure on the Si substrate, this amorphous oxide layer has to be removed. Here, an *in situ* cleaning process is of great advantage. For this purpose, the Si substrates have been laser heated in vacuum to $T_S = 900^\circ\text{C}$ with a rate of 100 K/min and subsequently up to 1150°C at 50 K/min. Then, the substrate was held for 10 min at this temperature. After that it was cooled down with a rate of 200 K/min to the deposition temperature of the first buffer layer (deposition of TiN at $T_S = 600^\circ$).

The whole high temperature treatment of the substrate

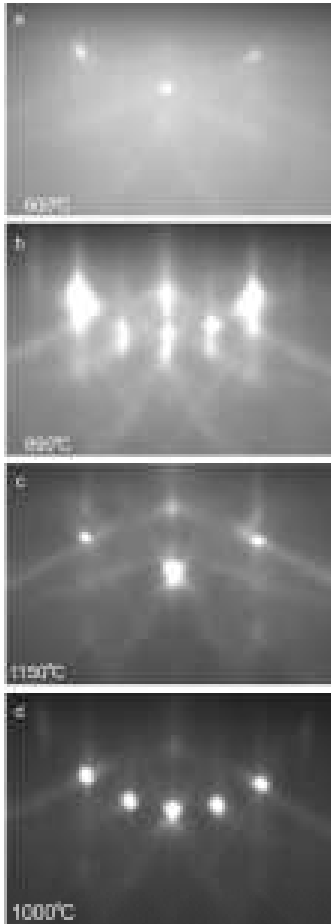


Figure 2: RHEED images taken at $[110]$ azimuth of the Si(001) substrate during the heat treatment. (a) Untreated substrate at $T_S = 600^\circ\text{C}$, (b) after heating to $T_S = 890^\circ\text{C}$, (c) at the maximum temperature of 1150°C , and (d) after cooling to $T_S = 1000^\circ\text{C}$.

surface was monitored by RHEED. The corresponding RHEED patterns are shown in Fig. 2. At low temperatures (Fig. 2a, $T_S = 600^\circ$), a large homogeneous background signal is visible due to diffuse scattering from the amorphous silicon oxide surface layer. Increasing the temperature, the signal from the (2×1) surface reconstruction becomes visible within a lightly streaky pattern at about $T_S = 900^\circ$ (Fig. 2b). The surface reconstruction takes place only after oxygen and other impurities such as SiC have desorbed from the surface. It is interesting to note, that at temperatures above 1100°C the (2×1) surface reconstruction disappears. A possible explanation is that the dimer bonds of the (2×1) surface displacement structure are dissolved at that temperature. Note that the diffuse background signal has disappeared, showing that the oxide has been completely removed from the substrate surface. After cooling down to 1000°C , a stable

and clean (2×1) surface is obtained with strong diffraction spots on the Laue circle of 0^{th} order, faint streaks, and Kikuchi lines. In summary, the process described above yields a clean Si(001) (2×1) surface, as indicated by the presence of the additional diffraction spots, without any chemical surface treatment.

EXPERIMENTAL RESULTS AND DISCUSSION

Epitaxial growth of TiN, MgO, and Fe_3O_4

For the pulsed laser deposition of the TiN, MgO, and Fe_3O_4 thin films we used a 248 nm KrF excimer laser with an energy density at the target of $2\text{--}5\text{ J/cm}^2$ per shot, and a pulse repetition rate of $2\text{--}10\text{ Hz}$, depending on the deposited material. Stoichiometric targets have been used for the growth of all films.

We first discuss the TiN films deposited in an Ar atmosphere of $2.5 \cdot 10^{-3}\text{ mbar}$ and a pulse repetition rate of 5 Hz . As a function of substrate temperature we have found two different growth modes of the TiN(001) films on the Si(001) surface that have been cleaned prior to deposition as described above. As demonstrated by the optical micrographs shown in Fig. 3, above about $T_S = 650^\circ\text{C}$ a three-dimensional Volmer-Weber (island) growth mode is obtained, whereas below this temperature a two-dimensional layer-by-layer growth mode is observed. For the Volmer-Weber growth mode the islands are oriented along the $[110]$ direction of the Si(001) substrate. The size of the mostly quadratic islands was about $3\text{ }\mu\text{m} \times 3\text{ }\mu\text{m}$. It is not obvious why in the temperature range above 650°C TiN grows with this preferential direction. We believe, that this is due to the 45° rotation of the dimer rows in the 2×1 surface reconstruction. With the lattice constant of Si (diamond structure, $a = 0.543\text{ nm}$) the distance of the Si atoms along the $[110]$ direction is $a/\sqrt{2} = 0.384\text{ nm}$ resulting in a considerable lattice mismatch of 9.4% to TiN (cubic, $a = 0.424\text{ nm}$). The transition into the island growth mode with increasing temperature itself is kinetic energy driven. For lower temperatures, a smooth two-dimensional growth mode is obtained. It is most likely that the growth occurs in the so-called 5-on-4-cube-on-cube bulk superstructure with a mismatch of about -2.4% [15, 16]. In this superstructure 5 TiN unit cells overlap 4 Si(100) unit cells.

The RHEED pattern recorded during the growth of the TiN films is shown in Fig. 4. During the first 70 to 140 laser pulses corresponding to a film thickness of about 0.4 nm to 0.8 nm , TiN grows in a smooth superstructure resulting in a rich diffraction pattern (see Fig. 4a). With increasing film thickness the fine structure in the RHEED pattern disappears and clear diffraction spots are observed at positions expected for small island transmission (see Fig. 4b). This is consistent with an *in situ* AFM analysis, which yields an average surface roughness

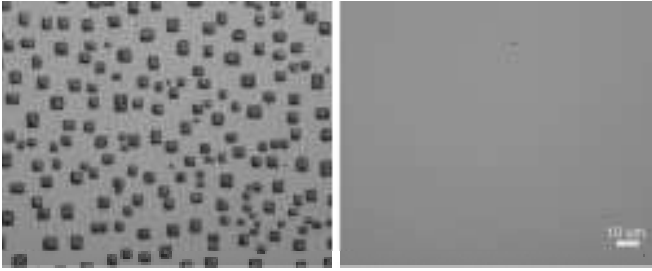


Figure 3: Optical micrographs of the surface of TiN films grown on Si(001). Left: Island growth mode at $T_S = 650^\circ\text{C}$. Right: Two-dimensional growth mode at $T_S = 600^\circ\text{C}$.

below 1 nm on a $1 \times 1 \mu\text{m}$ area at a film thickness of a few 10 nm.

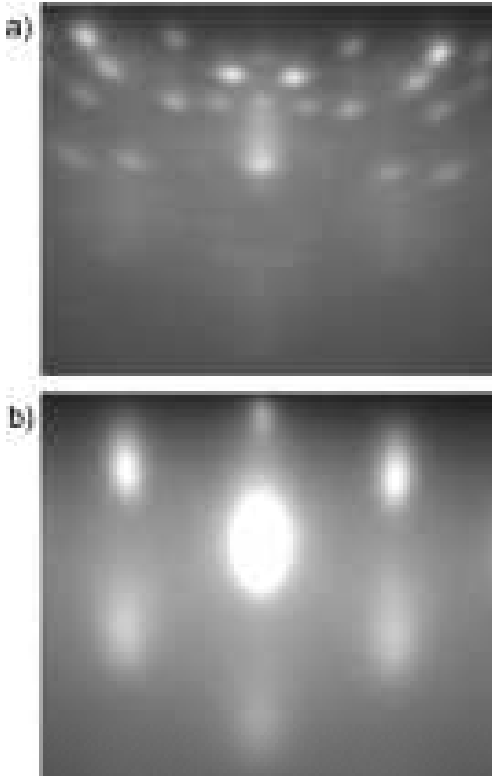


Figure 4: RHEED pattern recorded during the growth of a TiN film on a Si(001) substrate after 70 (a) and 1000 laser pulses (b). The deposition temperature was $T_S = 600^\circ\text{C}$.

After the growth of the TiN buffer layer the substrate temperature is lowered to $T_S = 330^\circ\text{C}$. Then, as a second buffer layer MgO is deposited at the same Ar pressure and a laser pulse repetition rate of 5 Hz. During the MgO growth the RHEED pattern becomes more streaky. This indicates a smoothening of the surface, which is consistent with *in situ* AFM measurements of the MgO surface. On a $1 \times 1 \mu\text{m}^2$ area of the MgO surface the average roughness was about 0.6 nm. This shows that MgO is well

suited as a buffer layer in the described system since it provides smooth interfaces, and therefore can also serve as insulator in a tunneling injection device.

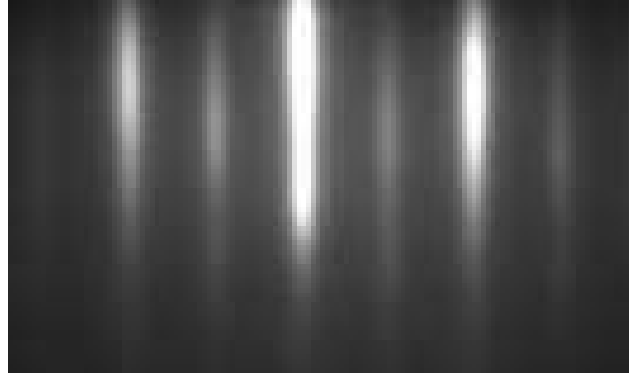


Figure 5: RHEED pattern recorded during the growth of Fe_3O_4 on the TiN/MgO buffer layer system after 5000 laser pulses corresponding to a thickness of the Fe_3O_4 film of about 40 nm.

On the completed TiN/MgO buffer layer system, an epitaxial magnetite film has been grown at $T_S = 330^\circ\text{C}$ also in the same Ar atmosphere of $2.5 \cdot 10^{-3}$ mbar, at a laser pulse repetition rate of 2 Hz. These parameters have been found to result in the best RHEED intensity oscillations due to a layer-by-layer growth of Fe_3O_4 on MgO substrates [17]. Note that the RHEED pattern recorded during the growth of the magnetite film (see Fig. 5) is streaky but shows no indication of any transmission spots suggesting a smooth surface in contrast to the TiN layer. The small roughness of the surface of the magnetite film has been demonstrated directly by *in situ* AFM measurements performed after deposition. For an area of $1 \times 1 \mu\text{m}^2$ a root mean square (rms) roughness of only 0.3 nm has been found. The stripes in the RHEED pattern obtained for magnetite have only about half the spacing of the diffraction spots obtained for TiN and MgO. This is caused by the fact that the lattice constant of magnetite is about twice the one of TiN and MgO (see Figs. 4 and 5).

During the growth of magnetite on the TiN/MgO buffer layer system RHEED oscillations could be observed as shown in Fig. 6. From the total number of RHEED oscillations, the number of laser pulses per single oscillation and the film thickness determined from x-ray reflectometry (see next section), we find that four RHEED oscillations are obtained during the growth of a single unit cell thick layer. That is, the magnetite unit cell grows in four sub-unit-cell blocks as discussed in detail elsewhere [17]. After the growth of several unit cells the amplitude of the RHEED oscillations decreases and finally vanishes due to surface roughening. However, after an annealing step at the deposition temperature, the RHEED intensity recovers to about the same value observed before starting the deposition process. A key re-

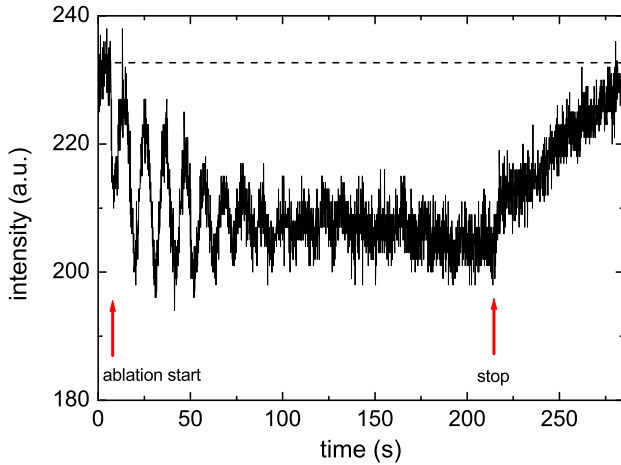


Figure 6: RHEED oscillations of the (0,1) diffraction spot recorded during the PLD growth of Fe_3O_4 on $\text{Si}(001)$ at $T_S = 330^\circ\text{C}$. The decay of the amplitude of the RHEED oscillations due to surface roughening and the recovery of the initial intensity after stopping the deposition process is clearly visible.

sult is that a layer-by-layer growth mode of Fe_3O_4 can be realized on the TiN/MgO buffer layer system on $\text{Si}(001)$ similar to the growth of Fe_3O_4 on MgO single crystalline substrates.

Structural analysis by HRXRD

The structural properties of the thin films and the quality of epitaxy have been characterized using a four circle x-ray diffractometer. We have used an x-ray mirror and an asymmetric fourfold monochromator. This is required to have sufficient intensity and resolution in order to be able to distinguish between the diffraction peaks of the different layers which are expected to be close together.

The upper panel of Fig. 7 shows a $\theta - 2\theta$ scan of the completed $\text{TiN}/\text{MgO}/\text{Fe}_3\text{O}_4$ multilayer system grown on $\text{Si}(001)$. All layers have been grown in the (00ℓ) orientation of the substrate yielding only (00ℓ) peaks. Within the resolution of our x-ray diffraction system, no peaks of other chemical phases could be detected. The detailed positions of the (00ℓ) peaks of the thin TiN and MgO buffer layers in the heterostructure are difficult to be determined (see lower panel of Fig. 7). Therefore, individual TiN films and TiN films with thicker MgO top layers have been grown for x-ray analysis. From these samples the following values for the c -axis parameter have been found: Fe_3O_4 : $c = 0.847\text{ nm}$, MgO : $c = 0.419\text{ nm}$, and TiN : $c = 0.420\text{ nm}$. The FWHM of the rocking curve of the magnetite (004) peak was about 0.7° . This value is about ten times larger than the value measured for Fe_3O_4 films grown directly on MgO substrates under sim-

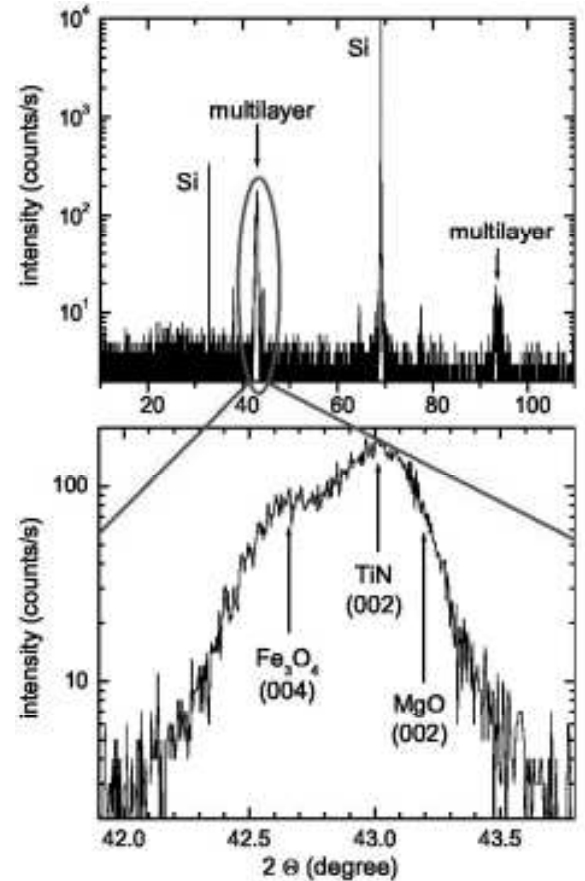


Figure 7: 2θ - ω x-ray scans of the $\text{TiN}/\text{MgO}/\text{Fe}_3\text{O}_4$ multilayer system grown on $\text{Si}(001)$. The unlabeled peaks are also found in the bare $\text{Si}(001)$ substrate. The lower panel shows part of the upper panel on an enlarged scale from about 41.9° to 43.8° .

ilar deposition conditions. This large difference can be attributed to the large lattice mismatch between Fe_3O_4 (as well as the TiN/MgO buffer layer) and Si compared to Fe_3O_4 and MgO (lattice mismatch of Fe_3O_4 : -2.4% on $\text{Si}(001)$ for the 5-on-4-cube-on-cube growth mode and only -0.31% on MgO). The large lattice mismatch results in strain relaxation effects and the formation of misfit dislocations increasing the mosaic spread of the films.

It is important to consider also the in-plane lattice constants in order to estimate whether or not the strain due to the lattice mismatch between the buffer layers and the substrate is (at least partially) relaxed. This can be done by several methods. A $2\theta - \chi$ mapping of the TiN (111) peak is shown in Fig. 8. Having determined the c -axis lattice parameter ($c = 0.420\text{ nm}$) from the $\theta - 2\theta$ scans, the in-plane lattice constant a can be calculated for the

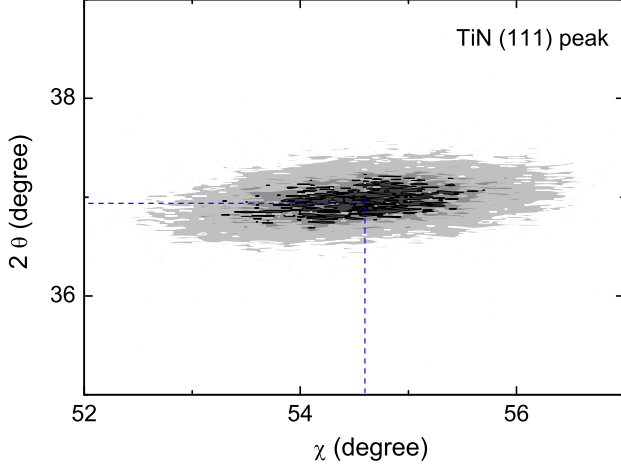


Figure 8: X-ray $2\theta - \chi$ mapping of the TiN (111) peak.

tetragonal lattice of TiN as

$$a = \sqrt{\frac{h^2 + k^2}{\left(\frac{2 \sin \theta}{\lambda}\right)^2 - \left(\frac{\ell}{c}\right)^2}}. \quad (1)$$

Here, h , k and ℓ are the Miller indices of the respective diffraction spot and λ the wavelength of the Cu-K $_{\alpha 1}$ x-ray radiation used for the experiment. With $c = 0.420$ nm, $h = k = \ell = 1$, $\theta = 36.97^\circ$ and $\lambda = 0.15418$ nm we obtain $a \simeq 0.422$ nm. This value is close to the bulk value of TiN ($a = 0.424$ nm). That is, most part of the TiN layer contributing to the intensity of the (111) peak is relaxed. From the mapping shown in Fig. 8 the in-plane lattice constant and the tetragonal distortion can be determined both from the θ -value using eq.(1) and the χ -value, which is given by the relation between the in-plane ($a = b$) and out-of-plane (c) lattice constants as

$$\frac{c\sqrt{2}}{a} = \tan \chi. \quad (2)$$

This relation directly follows from the symmetry of the tetragonal unit cell. For a nondistorted lattice (cubic symmetry), the χ -value should be 54.74° . As shown by Fig. 8, the measured value is 54.64° resulting in a c -axis parameter of 0.42 nm, which is consistent with the value determined from the $\theta - 2\theta$ scan. It is evident from Fig. 8 that the (111) peak is much broader in the χ than in 2θ direction. This is caused by the measuring geometry using a line profile of the x-ray beam. Analyzing the magnetite (113) peak, we have determined the in-plane lattice constants of magnetite to $a = b = 0.832$ nm by the same procedure. This value is close to the bulk value of $a = 0.835$ nm. We note that the relaxation of the TiN buffer layer allows the growth of an almost strain free magnetite layer on Si(001).

We also performed φ scans to check the epitaxial relations between the different layers and the substrate. We found that the (111) TiN, (113) magnetite, and (111) Si peak in a φ -scan (not shown) always appear at the same in-plane angle φ with the same fourfold symmetry. This shows that the in-plane lattice vectors of all layers are strictly aligned parallel to the Si substrate underlining the epitaxial nature of the obtained growth. We obtain the following epitaxial relations: $[100]_{Fe_3O_4} \parallel [100]_{MgO} \parallel [100]_{TiN} \parallel [100]_{Si}$.

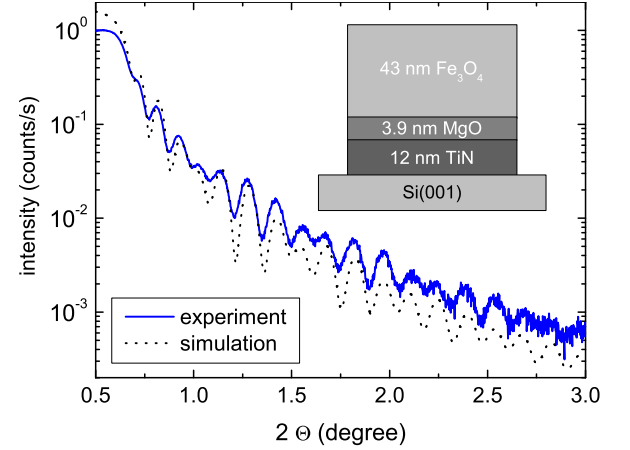


Figure 9: X-ray reflectometry data obtained for a TiN/MgO/Fe $_3$ O $_4$ multilayer system grown on Si(001). Also shown is the simulation result.

The thickness of the individual layers within the TiN/MgO/Fe $_3$ O $_4$ multilayer structure was determined by low angle x-ray reflectometry. The experimental results have been fitted using a simulation software based on dynamical scattering theory [18]. Fig. 9 shows a reflectometry measurement of a complete multilayer system consisting of a TiN/MgO/Fe $_3$ O $_4$ multilayer on Si(001). Note the convincing agreement between the simulation and the measurement of the complicated heterostructure. From the refinement the layer thickness in this example is obtained to 43 nm for magnetite, 3.9 nm for MgO, and 12 nm for TiN. By fitting the data also the roughness of the surface as well as of the interfaces between the layers and the substrate could be estimated. The derived roughness values are in the range between 0.3 and 0.7 nm. This is fully consistent with the roughness values obtained from the AFM analysis.

SUMMARY

Using pulsed laser deposition we have successfully grown magnetite epitaxial thin films on Si(001) substrates using a double buffer layer system consisting of TiN and MgO. For the reproducible cleaning of the Si substrate we have used an *in situ* laser heating process

with a maximum temperature of 1150°C. The substrate treatment and the whole growth process was monitored directly by RHEED allowing the determination of the surface structure at each process step. By x-ray diffraction and AFM, the good crystalline quality of the multilayers and the small roughness of the interfaces were verified. Due to their high Curie temperature and predicted large spin polarization magnetite thin films on Si substrates are highly interesting for potential applications in spintronics, in particular for spin injection into semiconductors. The compatibility of the presented multilayer structure with the insulating material MgO may provide a way to fabricate a suitable tunnel barrier to overcome the resistivity mismatch between ferromagnetic metals and semiconductors.

This work was supported in part by the Deutsche Forschungsgemeinschaft (project No.: Al/560) and the BMBF (project No.: 13N8279).

* Electronic address: Daniel.Reisinger@wmi.badw.de

† Electronic address: Lambert.Alff@wmi.badw.de

- [1] Z. Yu, J. Ramdani, J. A. Curless, C. D. Overgaard, J. M. Finder, R. Droopad, K. W. Eisenbeiser, J. A. Hallmark, W. J. Ooms, and V. S. Kaushik, *J. Vac. Sci. Technol. B* **18**, 2139 (2000).
- [2] S. Datta and B. Das, *Appl. Phys. Lett.* **56**, 665 (1990).
- [3] J. Kikkawa and D. D. Awschalom, *Nature (London)* **397**, 139 (1999).
- [4] R. Fiederling, M. Keim, G. Reuser, W. Ossau, G. Schmidt, A. Waag, and L. Molemkamp, *Nature (London)* **402**, 787 (1999).
- [5] Y. Ohno, D. K. Young, B. Beschoten, F. Matsukura, H. Ohno, and D. D. Awschalom, *Nature (London)* **402**, 790 (1999).
- [6] A. Gupta, J.Z. Sun, *J. Magn. Magn. Mat.* **24-43**, 200 (1999).
- [7] J. B. Philipp, J. Klein, D. Reisinger, M. Schonecke, A. Marx, A. Erb, L. Alff, and R. Gross, *Appl. Phys. Lett.* **79**, 3654 (2001).
- [8] G. Schmidt, D. Ferrand, L. W. Molemkamp, A. T. Filip, and B. J. Van Wees, *Phys. Rev. B* **62**, 4790 (2000).
- [9] E. Rashba, *Phys. Rev. B* **62**, R16267 (2000).
- [10] A. Fert and H. Jaffrès, *Phys. Rev. B* **64**, 184420 (2001).
- [11] R. Gross, J. Klein, B. Wiedenhorst, C. Höfener, U. Schoop, J. B. Philipp, M. Schonecke, F. Herbstritt, L. Alff, Yafeng Lu, A. Marx, S. Schymon, S. Thienhaus, W. Mader, in *Superconducting and Related Oxides: Physics and Nanoengineering IV*, D. Pavuna and I. Bosovic eds., SPIE Conf. Proc. **Vol. 4058** (2000), pp. 278–294.
- [12] J. Klein, C. Höfener, L. Alff, and R. Gross, *J. Magn. Magn. Mat.* **211**, 9 (2000); see also *Supercond. Sci. Technol.* **12**, 1023 (1999), and *Phys. Stat. Sol. (a)* **189**, No. 3, 617-620 (2002).
- [13] G. J. H. M. Rijnders, G. Koster, D. H. A. Blank, H. Rogalla, *Appl. Phys. Lett.* **70**, 1888 (1997).
- [14] S. Ohashi, M. Lippmaa, N. Nakagawa, H. Nagasawa, H. Koinuma and M. Kawasaki, *Rev. Sci. Instr.* **70**, 178 (1999).
- [15] R. Chowdury, X. Chen, J. Narayan, *Appl. Phys. Lett.* **64**, 1236 (1994).
- [16] P. R. Willmott, R. Timm, J. R. Huber, *Appl. Surf. Sci.* **127-129**, 105 (1998).
- [17] D. Reisinger, B. Blass, J. Klein, J. B. Philipp, M. Schonecke, A. Erb, L. Alff, and R. Gross, *cond-mat/0208495*, *Appl. Phys. A*, in print.
- [18] Bruker AXS Windows RefSim simulation software (based on dynamical scattering theory).